PROCEEDINGS OF SCIENCE

# Properties of Cosmic Deuterons Measured by the Alpha Magnetic Spectrometer

**Carlos Delgado**[a,*]

[a] *CIEMAT,*
*Avda. Complutense 40, Madrid, Spain*

*E-mail:* carlos.delgado@ciemat.es

Precision measurements of the cosmic ray D flux are presented as function of rigidity from 1.9 to 21 GV, based on 21 million D nuclei. We observed that over the entire rigidity range D exhibits nearly identical time variations with p, $^3$He, and $^4$He fluxes. Above 4.5 GV, the D/$^4$He flux ratio is time independent and its rigidity dependence is well described by a single power law $\sim R^{\Delta}$ with $\Delta_{D/^4He}$ = -0.108 ± 0.005. This is in contrast with the $^3$He/$^4$He flux ratio for which we find $\Delta_{^3He/^4He}$= -0.289 ± 0.003. The significance of $\Delta_{D/^4He} > \Delta_{^3He/^4He}$ exceeds $10\sigma$. In addition, we found that above $\sim$ 13 GV the rigidity dependence of D and p fluxes is identical with a D/p flux ratio of 0.027 ± 0.001. These unexpected observations show that, contrary to expectations, cosmic deuterons have a sizeable primary component.

*42nd International Conference on High Energy Physics (ICHEP2024)*
*18-24 July 2024*
*Prague, Czech Republic*

*Speaker





PoS(ICHEP2024)670

## 1. Introduction

Hydrogen nuclei are the most common species in cosmic rays.These nuclei include two stable isotopes: protons ($p$) and deuterons (D). Big Bang nucleosynthesis predicts minimal deuterium production, and over time, the abundance of D decreases from its primordial level. The observed D/$p$ ratio in the interstellar medium is approximately $2 \times 10^{-5}$ [1]. Unlike primary cosmic rays such as $p$ and $^4$He, which are accelerated in supernova remnants, deuterons are mainly produced by He interactions with the interstellar medium. Deuterons, along with $^3$He, are classified as secondary cosmic rays, and previous research has shown that these cosmic rays, including Li, Be, and B, share a similar rigidity dependence [2–4].

The interaction cross sections of deuterons and He with the interstellar medium are significantly lower than those of heavier nuclei [5]. Specifically, the D/$^4$He and $^3$He/$^4$He flux ratios provide insight into diffusion properties at larger distances than those probed by heavier nuclei. These measurements are crucial for refining cosmic ray propagation models [6–11].

## 2. AMS Detector

The layout of the detector is shown in Fig. 1 (left). The key elements are the permanent magnet [12], the silicon tracker [13], four planes of time of flight (TOF) scintillation counters [14], the array of anticoncidence counters (ACCs) [15], the transition radiation detector (TRD) [16], the ring imaging Čerenkov detector (RICH) [17], and the electromagnetic calorimeter (ECAL) [18]. The AMS coordinate system is concentric with the magnet. The $x$ axis is parallel to the main component of the magnetic field. The ($y$-$z$) plane is the bending plane. Above, below, and downward- going refer to the AMS coordinate system. The central field of the magnet is 1.4 kG. On orbit, the magnet temperature varies from −3 to +20°C. The field strength is corrected with a measured temperature dependence of −0.09%/°C.

The tracker has nine layers, the first ($L1$) at the top of the detector, the second ($L2$) just above the magnet, six ($L3$ to $L8$) within the bore of the magnet, and the last ($L9$) just above the ECAL. $L2$ to $L8$ constitute the inner tracker.The tracker accurately determines the trajectory of cosmic rays by multiple measurements of the coordinates with a resolution in each layer of 5–10 $\mu$m in the bending ($y$) direction for different nuclei [19]. Together, the tracker and the magnet measure the rigidity $R$ of charged cosmic rays, with a maximum detectable rigidity of up to 3.5 TV.Each layer of the tracker provides an independent measurement of the charge $Z$ with a resolution.Overall, the inner tracker has a resolution of $0.05 < \sigma_Z < 0.3$ for Z=1...28 [20].

As seen from Fig. 1 (left), two of the TOF planes are located above the magnet (upper TOF) and two planes are below the magnet (lower TOF). The overall velocity ($\beta = v/c$) resolution has been measured to be $\sigma(1/\beta) = 0.01 - 0.04$ for different nuclei.The pulse heights of the upper and lower planes each provide independent charge measurements with an accuracy of $\sigma_Z/Z \sim 2$

The RICH is located below the two lower TOF planes. Its radiator is located at its top, which is made of two non-overlapping dielectric materials. The radiator consists of tiles of silica aerogel with a refraction index of 1.05 and, in the central part, of tiles of sodium fluoride with a refraction index of 1.33. Its velocity resolution has been measured to be $\sigma(\beta)/\beta = 1.3 \times 10^{-3}$ for charge 1 particles crossing the aerogel radiator, and $\sigma(\beta)/\beta = 3.2 \times 10^{-3}$ for the sodium fluoride one.

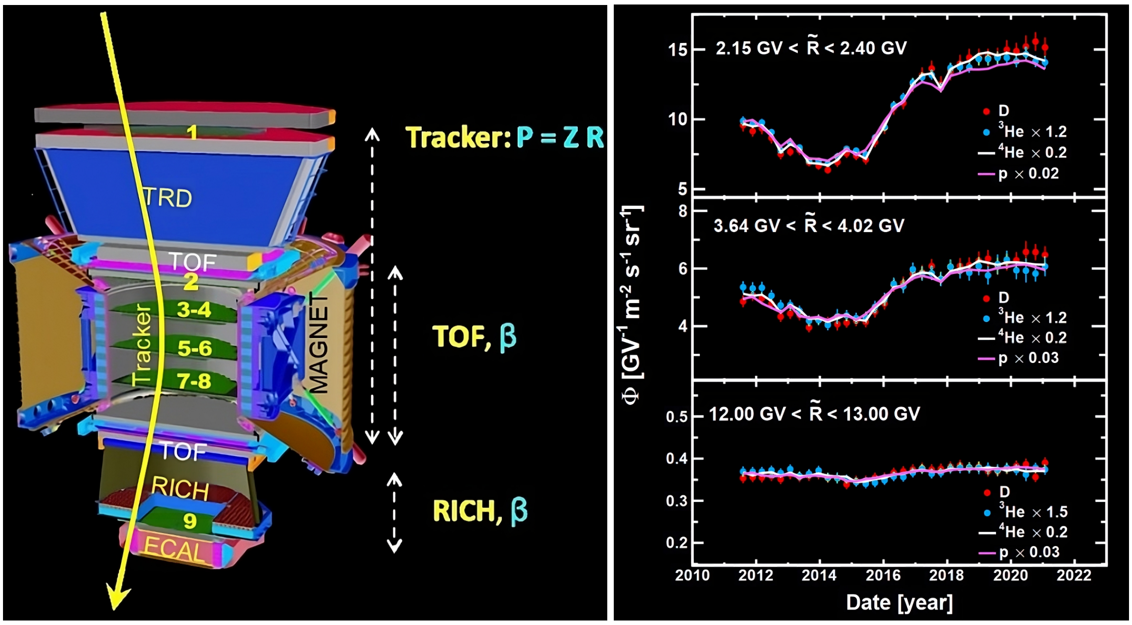


**Figure 1:** (left) The AMS detector showing the main elements and their functions. (right) The AMS D (red points), $^3$He (blue points), $^4$He (white curves), and $p$ (magenta curves) fluxes as functions of time for three characteristic rigidity bins.

Monte Carlo (MC) simulated events were produced using a dedicated program developed by the collaboration based on the GEANT4-10.3 package [21]. The program simulates electromagnetic and hadronic interactions [22] of particles and nuclei in the material of AMS and generates detector responses.The simulated events then undergo the same reconstruction as used for the data.

## 3. Results

The deuteron (D) fluxes were measured as a function of rigidity from May 2011 to April 2021. To facilitate a comparison of the temporal and rigidity dependence of the D fluxes with those of $^3$He and $^4$He, the $^3$He and $^4$He measurements from Ref.[23] were extended to April 2021 and to the rigidity range of 1.9 to 21 GV.

Figure 1 (right) shows the AMS D flux as a function of time for three characteristic rigidity bins, compared with the AMS $p$, $^3$He, and $^4$He fluxes. The $p$ fluxes were extracted from Ref. [24], with the D fluxes subtracted. All these spectra exhibit nearly identical variations with time and the relative magnitude of the variations decreases with increasing rigidity. To study the time variation of the D flux in detail, we fit a linear relation between the relative variations of $\Phi_{\mathrm{D}}/\Phi_{^4\mathrm{He}}$ and of $\Phi_{^4\mathrm{He}}$ for each rigidity bin $i$, as of:

$$\frac{\Phi^i_{\mathrm{D}}/\Phi^i_{^4\mathrm{He}} - \langle \Phi^i_{\mathrm{D}}/\Phi^i_{^4\mathrm{He}} \rangle}{\langle \Phi^i_{\mathrm{D}}/\Phi^i_{^4\mathrm{He}} \rangle} = k^i_{\mathrm{D}} \frac{\Phi^i_{^4\mathrm{He}} - \langle \Phi^i_{^4\mathrm{He}} \rangle}{\langle \Phi^i_{^4\mathrm{He}} \rangle} \tag{1}$$

where $k^i_{\mathrm{D}}$ is the slope of the linear dependence for the rigidity bin $i$. Figure 2 shows that the slope $k$D, as a function of the rigidity from 1.9 to 7.8 GV, is compatible with zero above 4.5 GV.

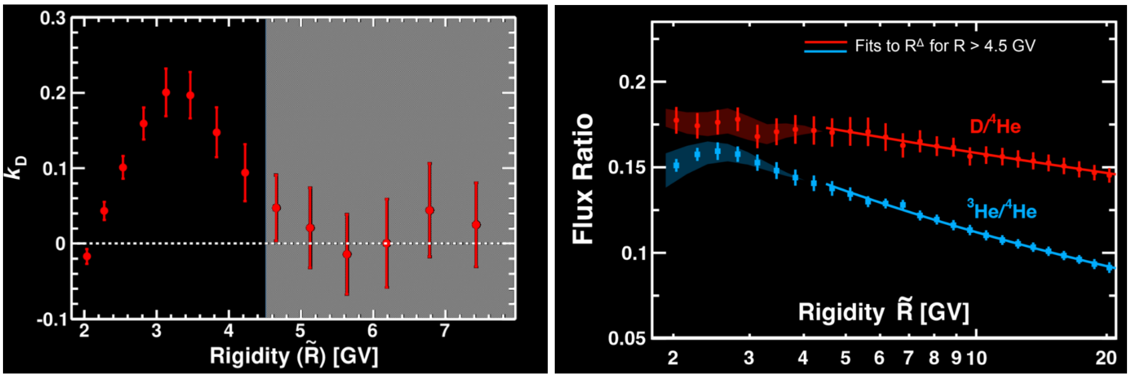


**Figure 2:** (left) The slope of the linear fit of $\Phi_D/\Phi_{^4He}$ versus rigidity. The shaded area indicates the rigidity range where the slope is statistically consistent with zero. (right) The time-averaged flux ratios, D/$^4$He (red circles) and $^3$He/$^4$He (blue squares), are plotted as a function of rigidity with total errors. The red and blue lines represent power-law fits for $R > 4.5$ GV.

The time-averaged flux ratios of D/$^4$He and $^3$He/$^4$He as functions of rigidity are presented in Fig. 2 (right). For rigidities above 4.5 GV, these ratios follow a power law of the form $C, (R/4.5, \text{GV})^{\Delta}$. For the D/$^4$He flux ratio, a fit to the data yields: $\Delta_{D/^4He} = -0.108 \pm 0.005$. For the $^3$He/$^4$He flux ratio, the fit results in $\Delta_{^3He/^4He} = -0.289 \pm 0.003$. The spectral index for the D/$^4$He flux ratio differs from that of $^3$He/$^4$He. The condition $\Delta_{D/^4He} > \Delta_{^3He/^4He}$ is confirmed with a significance greater than $10\sigma$. This suggests that cosmic deuterons contain a substantial component with a primary-like spectrum.

We estimate the primary ($\Phi_D^P$) and secondary ($\Phi_D^S$) components of the deuterium flux ($\Phi_D$) by fitting $\Phi_D = \Phi_D^P + \Phi_D^S$ to a weighted combination of a typical primary cosmic ray flux ($\Phi_{^4He}$) and a typical secondary cosmic ray flux ($\Phi_{^3He}$) above 4.5 GV. The fitting results in $\Phi_D^P = (0.094 \pm 0.005) \times \Phi_{^4He}$ and $\Phi_D^S = (0.58 \pm 0.05) \times \Phi_{^3He}$ as displayed in Fig. 3.

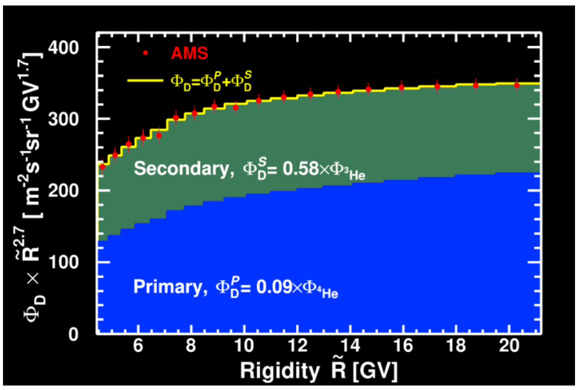


**Figure 3:** The time-averaged $\Phi_D$ (red circles) multiplied by $\tilde{R}^{2.7}$ as a function of rigidity with total errors above 4.5 GV together with the fit to the weighted sum of $\Phi_{^4He}$ and $\Phi_{^3He}$(yellow curve). The contributions of the primary and secondary components are indicated by the blue and green shadings, respectively.

## 4. Discussion

We reported the precision measurements of the cosmic ray deuteron (D) flux in the rigidity range from 1.9 to 21 GV. Across this range, the D flux exhibits time variations nearly identical to those of the proton, $^3$He, and $^4$He fluxes. Above 4.5 GV, the rigidity dependence of the flux ratio D/$^4$He follows a single power law, $\propto R^{\Delta}$, with $\Delta_{\mathrm{D}/^4\mathrm{He}} = -0.108 \pm 0.005$, different from the $^3$He/$^4$He ratio, where $\Delta_{^3\mathrm{He}/^4\mathrm{He}} = -0.289 \pm 0.003$. The difference between $\Delta_{\mathrm{D}/^4\mathrm{He}}$ and $\Delta_{^3\mathrm{He}/^4\mathrm{He}}$ is statistically significant, exceeding 10 $\sigma$. These findings suggest the presence of a primary-like component in cosmic deuterons, contrary to prior expectations. Using a method independent of cosmic ray propagation models, we estimate the primary component of the D flux to be $9.4 \pm 0.5\%$ of the $^4$He flux, and the secondary component to be $58 \pm 5\%$ of the $^3$He flux.

## References

[1] S. D. Friedman *et al.*, A High-precision Survey of the D/H Ratio in the Nearby Interstellar Medium, Astrophys. J. **946**, 34 (2023);

[2] B. Coste, L. Derome, D. Maurin, and A. Putze, Constraining Galactic cosmic-ray parameters with $Z \leq 2$ nuclei, Astron. Astrophys. **539**, A88 (2012).

[3] I. A. Grenier, J. H. Black and A. W. Strong, The Nine Lives of Cosmic Rays in Galaxies, Annu. Rev. Astron. Astrophys. **53**, 199 (2015); P. Blasi, The origin of galactic cosmic rays, Astron. Astrophys. Rev. **21**, 70 (2013); A. W. Strong, I. V. Moskalenko, and V. S. Ptuskin, Cosmic-Ray Propagation and Interactions in the Galaxy, Annu. Rev. Nucl. Part. Sci. **57**, 285 (2007).

[4] M. Aguilar *et al.*, Observation of New Properties of Secondary Cosmic Rays Lithium, Beryllium, and Boron by the Alpha Magnetic Spectrometer on the International Space Station, Phys. Rev. Lett. **120**, 021101 (2018).

[5] Y. Génolini, D. Maurin, I. V. Moskalenko, and M. Unger, Current status and desired precision of the isotopic production cross sections relevant to astrophysics of cosmic rays: Li, Be, B, C, and N, Phys. Rev. C **98**, 034611 (2018).

[6] N. Tomassetti, Propagation of H and He cosmic ray isotopes in the Galaxy: astrophysical and nuclear uncertainties, Astrophys. Space Sci. **342**, 131 (2012).

[7] G. Jóhannesson *et al.*, Bayesian analysis of cosmic ray propagation: Evidence against homogeneous diffusion, Astrophys. J. **824**, 16 (2016).

[8] A. W. Strong and I. V. Moskalenko, Propagation of Cosmic-Ray Nucleons in the Galaxy, Astrophys. J. **509**, 212 (1998).

[9] C. Evoli, D. Gaggero, A. Vittino, G. Di Bernardo, M. Di Mauro, A. Ligorini, P. Ullio, and D. Grasso, Cosmic-ray propagation with DRAGON2: I. numerical solver and astrophysical ingredients, J. Cosmol. Astropart. Phys. **02**, 015 (2017).

PoS(ICHEP2024)670

[10] D. Maurin, F. Donato, R. Taillet, and P. Salati, Cosmic Rays below Z = 30 in a Diffusion Model: New Constraints on Propagation Parameters, Astrophys. J. **555**, 585 (2001).

[11] A. Putze, L. Derome, and D. Maurin, A Markov Chain Monte Carlo technique to sample transport and source parameters of Galactic cosmic rays II. Results for the diffusion model combining B/C and radioactive nuclei, Astron. Astrophys. **516**, A66 (2010).

[12] K. Lübelsmeyer *et al.*, Nucl. Instrum. Methods Phys. Res., Sect. A **654**, 639 (2011).

[13] B. Alpat *et al.*, Nucl. Instrum. Methods Phys. Res., Sect. A **613**, 207 (2010).

[14] V. Bindi *et al.*, Nucl. Instrum. Methods Phys. Res., Sect. A **743**, 22 (2014).

[15] Ph. von Doetinchem *et al.*, Nucl. Phys. B, Proc. Suppl. 197, 15 (2009).

[16] Th. Kirn, Nucl. Instrum. Methods Phys. Res., Sect. A 706, 43 (2013).

[17] M. Aguilar et al., Nucl. Instrum. Methods Phys. Res., Sect. A 614, 237 (2010); F. Giovacchini Nucl. Instrum. Methods Phys. Res., Sect. A 766, 57 (2014).

[18] C. Adloff *et al.*, Nucl. Instrum. Methods Phys. Res., Sect. A 714, 147 (2013).

[19] G. Ambrosi, V. Choutko, C. Delgado, A. Oliva, Q. Yan, and Y. Li, Nucl. Instrum. Methods Phys. Res., Sect. A **869**, 29 (2017).

[20] Y. Jia, Q. Yan, V. Choutko, H. Liu, and A. Oliva, Nucl. Instrum. Methods Phys. Res., Sect. A **972**, (2020).

[21] J. Allison *et al.*, Nucl. Instrum. Methods Phys. Res., Sect. A **835**, 186 (2016); J. Allison *et al.*, IEEE Trans. Nucl. Sci. **53**, 270 (2006); S. Agostinelli *et al.*, Nucl. Instrum. Methods Phys. Res., Sect. A **506**, 250 (2003).

[22] Q. Yan, V. Choutko, A. Oliva, and M. Paniccia, Nuclear Physics A **996** 121712 (2020).

[23] M. Aguilar *et al.*, Properties of Cosmic Helium Isotopes Measured by the Alpha Magnetic Spectrometer, Phys. Rev. Lett. **123**, 181102 (2019).

[24] M. Aguilar *et al.*, Periodicities in the Daily Proton Fluxes from 2011 to 2019 Measured by the Alpha Magnetic Spectrometer on the International Space Station from 1 to 100 GV, Phys. Rev. Lett. **127**, 271102 (2021). The new $\Phi_p$ data up to April 2021 will be published separately.